JOURNAL OF AIRCRAFT
Vol. 37, No. 1, January–February 2000

Nonlinear Aeroelastic Response of Delta Wing to Periodic Gust

Deman Tang,* James K. Henry,† and Earl H. Dowell‡
Duke University, Durham, North Carolina 27708-0300

A nonlinear response analysis of a simple delta wing excited by periodic gust loads in low subsonic flow is presented along with a companion wind-tunnel test program. The analytical model uses a three-dimensional time-domain vortex lattice aerodynamic method and a reduced order aerodynamic technique. Results for a single harmonic gust and a continuous frequency sweep gust have been computed and measured for both flow velocities below and above the flutter speed. A theoretical jump response phenomenon for the nonlinear structural model was observed both for the single harmonic and the continuous frequency sweep gust excitation. Those results further confirm some conclusions about limit cycle oscillations above the flutter speed and complement our earlier theoretical and experimental studies. Also an experimental investigation has been carried out in the Duke wind tunnel using a rotating slotted cylinder gust generator and an Ometron VPI 4000 scanning laser vibrometer measurement system. The fair to good quantitative agreement between theory and experiment verifies that the present analytical approach has reasonable accuracy and good computational efficiency for nonlinear gust response analysis in the time domain. Without the use of reduced order models, calculations of the gust response for the nonlinear model treated here would be impractical.

Nomenclature

a_i, b_j	= generalized coordinates in x and y directions, respectively
c	= delta wing root chord
D	= delta wing plate bending stiffness
E	= Young's modulus
h	= delta wing plate thickness
km, kn	= numbers of vortex elements on delta wing in x and y directions, respectively
kmm	= total number of vortices on both the delta wing and wake in the x direction
L	= delta wing span
m	= delta wing panel mass/area, $h\rho_m$
mxy	= number of delta wing modal functions in the x and y planes defining u and v
nxy	= number of delta wing modal functions in the z direction defining w
Q^{ij}	= generalized aerodynamic force
$\boldsymbol{q}$, $\dot{\boldsymbol{q}}$	= state space vector
q_n	= generalized coordinate in the z direction
R_a	= size of reduced order aerodynamic model
R_x, R_y, R_z	= rotational deflections in x, y, and z directions
t	= time
U	= airspeed
U_F	= critical flutter velocity
U_i, V_j	= modal functions in x and y directions
u, v	= in-plane displacements
W_k	= transverse modal function in z direction
w	= plate transverse deflection
w_g, w_{g0}	= nondimensional lateral gust velocity and amplitude
X, Y	= right and left eigenvector matrices of vortex lattice eigenvalue model
x, y	= streamwise and spanwise coordinates
Z	= eigenvalue matrix of vortex lattice aerodynamic model
z	= normal coordinate
Γ	= vortex strength
Δp	= aerodynamic pressure loading on panel
$\overline{\Delta p}$	= nondimensional aerodynamic pressure, $\Delta p/(\rho_\infty U^2)$
Δt	= time step, $\Delta x/U$
Δx	= plate element length in the streamwise direction
θ	= state space vector
ν	= Poisson's ratio
ρ_∞, ρ_m	= air and plate densities
τ	= time parameter, $\sqrt{(mc^4/D)}$, s
ω	= frequency
$\cdot$	= d( )/dt

Introduction

THE study of atmospheric turbulence and its influence on aircraft operation and design has been of concern to many investigators. Areas of interest have included the measurement and modeling of atmospheric turbulence, as well as the response and structural design of aircraft encountering such turbulence or gusts. In the late 1980s, the Federal Aviation Administration requested assistance from NASA for initial evaluation of a candidate method for analysis of gust loads on aircraft with nonlinearities. The statistical discrete gust (SDG) method[1] has been proposed to permit analysis of nonlinear aircraft models for gust loads. As a time-domain method, it would also permit the computation of time-correlated gust loads. NASA conducted an evaluation of the SDG method, focusing on its relationship to existing linear methods.[2]

Recently, a three-dimensional time-domain vortex lattice aerodynamic model and reduced order aerodynamic technique was used[3,4] to investigate the flutter and limit cycle oscillation (LCO) characteristics of cantilevered low aspect ratio, rectangular and delta wing–plate structure models at low subsonic flow speeds. It has been shown that for a plate restrained at its root, bending/tension or geometrical nonlinearities can produce LCO amplitudes of the order of the plate thickness. A wind-tunnel model has been tested to provide a quantitative experimental correlation with the theoretical results for the LCO response itself.[5] In the present paper this method is extended to calculate and measure gust response when the time-correlated gust loads are known.

A few years ago, a rotating slotted cylinder (RSC) gust generator was installed in the Duke University low-speed wind tunnel and was used to generate a gust excitation field including a sinusoidal gust or a linear frequency sweep gust excitation.[6] This gust field can also

Received 26 October 1998; revision received 12 July 1999; accepted for publication 13 July 1999.

*Research Associate, Department of Mechanical Engineering and Materials Science.
†Research Assistant, Department of Mechanical Engineering and Materials Science.
‡J. A. Jones Professor and Dean, School of Engineering.

simulate turbulence with a uniform power spectral density over a certain frequency band in the lateral and longitudinal directions.[7,8]

Following the work of Ref. 5, in the present paper we develop a mathematical model and computational code in the time domain to calculate the nonlinear gust response of a delta wing model at low subsonic flow speeds. Sinusoidal and linear frequency sweep gust loads are used. To validate the theoretically predicted gust response characteristics of the delta wing, an experimental investigation has been carried out in the Duke University wind tunnel using an RSC gust generator and an Ometron VPI 4000 scanning laser vibrometer measurement system[9] to measure deflections (velocities) of the delta wing. The results may be helpful in better understanding physically the nonlinear aeroelastic response of a delta wing model to gust loads.

State-Space Equations

A schematic of the delta wing-plate geometry with a three-dimensional vortex lattice model of the unsteady flow is shown in Fig. 1. The aeroelastic structure/fluid state-space equations are described as follows.

Nonlinear Structural Equations

The nonlinear structural equations were derived from Hamilton's principle and the Lagrange equations based on the von Kármán plate equations using the total kinetic and elastic energies and the work done by applied aerodynamic loads on the plate. Modal expansions for the plate deflection are substituted into the energy expressions and then into Lagrange's equations to yield equations of motion for each structural modal coordinate. As is well known, von Kármán's plate equations take into account the nonlinear coupling between in-plane and out-of-plane plate motion as a result of retaining quadratic terms in the strain–displacement equations. Physically there is a stiffening of the plate due to an in-plane tension that increases quadratically with increasing out-of-plane displacement.

We expand the transverse or out-of-plane displacement w and the in-plane displacements u and v as follows:

$$u = \sum_i a_i(t)U_i(x, y) \tag{1}$$

$$v = \sum_j b_j(t)V_j(x, y) \tag{2}$$

$$w = \sum_k q_k(t)W_k(x, y) \tag{3}$$

where the transverse natural mode function $W_k(x, y)$ is calculated using a two-dimensional finite element method for the delta wing plate based on a standard computational code. The in-plane natural mode functions $U_i(x, y)$ and $V_j(x, y)$ are calculated using a three-dimensional finite element method for the delta wing. In this latter computational model, the transverse displacement w is constrained, and only the in-plane mode functions are extracted. These functions satisfy the boundary conditions of the cantilevered delta wing.

Here, a_i, b_j, and q_k are normalized by the plate thickness h and x and y by c and L, respectively.

It is assumed that all of the nonconservative forces act in the z direction only and the in-plane inertia may be neglected. Thus, the in-plane equations of motion are determined from the stretching strain energy and Lagrange's equation. The nondimensional in-plane (u, v) equations are then

$$\sum_p C_p^j a_p + \sum_g C_g^j b_g = C^j \tag{4}$$

$$\sum_p D_p^s a_p + \sum_g D_g^s b_g = D^s \tag{5}$$

where C^j and D^s are nonlinear (quadratic) functions of the delta wing transverse deflection. For details of the coefficient terms C_p^j, C_g^j, D_p^s, and D_g^s and the terms C^j and D^s, see Ref. 5.

The transverse equation is formed by substituting the kinetic, bending, and stretching energy expressions into Lagrange's equation. The nondimensional equation is

$$\sum_m A_m^k\left[\ddot{q}_m + 2\omega_m\xi_m\dot{q}_m + \omega_m^2 q_m\right] + \frac{F_N^k}{\tau^2} + \frac{Q^k}{\tau^2} = 0 \tag{6}$$

where A_m^k are constant coefficient terms and F_N^k is a (nondimensional) nonlinear force that depends on the deflection of the plate (for details, also see Ref. 5). Note that ξ_m and ω_m are the mth structural modal damping and natural frequency. Q^k is the nondimensionalized generalized aerodynamic force see [Eq.(12)]. We will discuss it next.

Aerodynamic Equations: Vortex Lattice Model

We assume that a spanwise uniform periodic lateral gust is used, that is, the gust velocity is only a function of chordwise position and time, $w_g = w_g(x, t)$, and it is normalized by airspeed U. The gust wavelength is defined as

$$l_g = U/\omega$$

where ω is the gust excitation frequency in hertz.

A continuous sinusoidal gust time history at the x_i position on the delta wing may be expressed as follows:

$$w_g(x, t) = w_{g0}\sin(2\pi\omega t - \Delta\phi) \tag{7}$$

where a phase difference is defined as $\Delta\phi = 2\pi x_i/l_g$.

A continuous frequency sweep gust is also considered. It is expressed as

$$w_g(x, t) = w_{g0}\sin\left[2\pi\omega_1 + \frac{2\pi(\omega_2 - \omega_1)}{2T}t^2 - \Delta\phi\right] \tag{8}$$

where ω_1, ω_2, and T are the minimum frequency, maximum frequency, and the sweep duration respectively.

The flow about the cantilever plate is assumed to be incompressible, inviscid, and irrotational. We use an unsteady vortex lattice

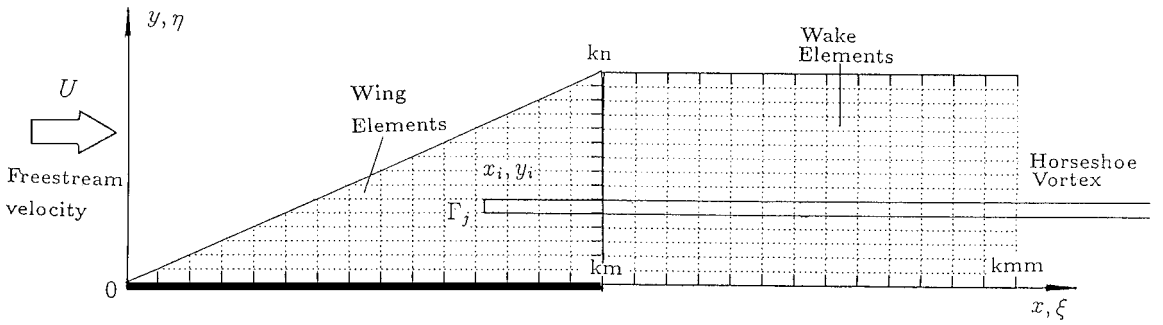

Fig. 1 Aeroelastic model of a delta wing; aerodynamic vortex lattice grid is shown, a finite element grid for the structural model is also used.

method to model this flow. A typical planar vortex lattice mesh for the three-dimensional flow is shown in Fig. 1. The delta wing and wake are divided into a number of elements. In the wake and on the wing, all of the elements are of equal size, Δx, in the streamwise direction. Point vortices are placed on the plate and in the wake at the quarter chord of the elements. At the three-quarter chord of each plate element, a collocation point is placed for the downwash, that is, we require the velocity induced by the discrete vortices to equal the total downwash arising from the unsteady motion of the delta wing and also the gust. Thus, we have the relationship

$$w_i^{t+1} = \sum_j^{kmm} K_{ij}\Gamma_j^{t+1} + w_{g,i}^{t+1} \qquad i = 1, \ldots, km \tag{9}$$

where w_i^{t+1} is the total downwash at the ith collocation point at time step $t+1$, Γ_j is the strength of the jth vortex, and K_{ij} is an aerodynamic kernel function. As described in Ref. 4, an aerodynamic matrix equation is given by

$$A\boldsymbol{\Gamma}^{t+1} + B\boldsymbol{\Gamma}^{t} = \boldsymbol{w}^{t+1} \tag{10}$$

where A and B are aerodynamic coefficient matrices.

From the fundamental aerodynamic theory, the nondimensional pressure is given by

$$\overline{\Delta p_j} = \frac{c}{\Delta x}\left[\frac{\Gamma_j^{t+1} + \Gamma_j^t}{2} + \sum_i^j (\Gamma_i^{t+1} - \Gamma_i^t)\right] \tag{11}$$

and the aerodynamic generalized force is calculated from

$$Q^k = \frac{\rho_\infty U^2 c^4}{Dh}\int_0^1\int_0^1 \overline{\Delta p} W_k \, \mathrm{d}x \, \mathrm{d}y \tag{12}$$

Aeroelastic State-Space Equations

Consider a discrete time history of the delta wing, $\boldsymbol{q}(t)$, with a constant sampling time step Δt. The sampled version of $\boldsymbol{q}(t)$ is then defined by

$$\boldsymbol{q} = (\boldsymbol{q}^{t+1} + \boldsymbol{q}^t)/2$$

and the velocity of this discrete time series is defined by

$$\dot{\boldsymbol{q}} = (\boldsymbol{q}^{t+1} - \boldsymbol{q}^t)/\Delta t$$

The structural dynamic equations (6) can be reconstituted as a state-space equation in discrete time form, that is,

$$D_2\theta^{t+1} + D_1\theta^t + C_2\boldsymbol{\Gamma}^{t+1} + C_1\boldsymbol{\Gamma}^t = -\boldsymbol{F}_N^{t+\frac{1}{2}} \tag{13}$$

where the vector θ is the state of the plate, $\{\theta\} = \{\dot{q}, q\}$, and D_1 and D_2 are matrices describing the plate structural behavior. C_1 and C_2 are matrices describing the vortex element behavior on the delta wing itself.

There is a linear relationship between the downwash w at the collocation points due to wing motion and the delta wing response θ. It is defined by

$$\boldsymbol{w} = E\theta \tag{14}$$

In addition, of course, there is a downwash due to the gust given by Eq. (7) or Eq. (8). Thus, we obtain a complete aeroelastic state-space equation in matrix form,

$$\begin{bmatrix} A & -E \\ C_2 & D_2 \end{bmatrix}\begin{Bmatrix} \Gamma \\ \theta \end{Bmatrix}^{t+1} + \begin{bmatrix} B & 0 \\ C_1 & D_1 \end{bmatrix}\begin{Bmatrix} \Gamma \\ \theta \end{Bmatrix}^{t} = \begin{Bmatrix} w_g^{t+1} \\ -F_N^{t+\frac{1}{2}} \end{Bmatrix} \tag{15}$$

Reduced Order Aerodynamic Model

If we assume the structural response to be zero and no gust excitation, then from Eq. (10) one obtains a representation of unforced fluid motion,

$$A\boldsymbol{\Gamma}^{t+1} + B\boldsymbol{\Gamma}^t = 0 \tag{16}$$

From Eq. (16), an aerodynamic eigenvalue problem may be formed. Because the matrices A and B are nonsymmetric, we must compute the right and left eigenvalues and eigenvectors of the generalized eigenvalue problem.

Let X and Y be the right and left eigenvector matrices, and Z is a diagonal matrix whose diagonal entries contain the eigenvalues. The right and left eigenvectors are orthogonal with respect to the matrices A and B. We normalize the eigenvectors such that they are orthonormal with respect to A.

Let the point vortex vector $\boldsymbol{\Gamma}$ be a linear combination of the R_a right eigenvectors (where usually in practice $R_a \ll$ total number of aerodynamic eigenvalues), that is,

$$\boldsymbol{\Gamma} = X_{Ra}\boldsymbol{\gamma}$$

where $\boldsymbol{\gamma}$ is the vector of the aerodynamic modal coordinates. To account for the neglected eigenmodes, therefore, we use a quasi-static correction that accounts for much of their influence. Let

$$\boldsymbol{\Gamma} = \boldsymbol{\Gamma}_s + \boldsymbol{\Gamma}_d = \boldsymbol{\Gamma}_s + X_{Ra}\boldsymbol{\gamma}_d$$

where the first term on the right-hand side is a quasi-static solution of the vortex flow and the second term is a dynamic perturbation solution. By definition, the quasi-static portion $\boldsymbol{\Gamma}_s$ is given by

$$[A + B]\boldsymbol{\Gamma}_s^t = \boldsymbol{w}^t + \boldsymbol{w}_g^t \tag{17}$$

where $\boldsymbol{w}^t$ and $\boldsymbol{w}_g^t$ are the downwashes at time step t. Compare Eqs. (10) and (17). Note Eq. (17) may be inverted once to determine $\boldsymbol{\Gamma}_s^t$ in terms of $\boldsymbol{w}^t + \boldsymbol{w}_g^t$ and does not need to be evaluated at each time step.

Thus, the reduced order model with static correction is given by

$$\begin{bmatrix} I & -Y_{Ra}^T[I - A(A+B)^{-1}]E \\ C_2X_{Ra} & D_2 + C_2(A+B)^{-1}E \end{bmatrix}\begin{Bmatrix} \gamma_d \\ \theta \end{Bmatrix}^{t+1} + \begin{bmatrix} -Z_{Ra} & +Y_{Ra}^T B(A+B)^{-1}E \\ C_1X_{Ra} & D_1 + C_1(A+B)^{-1}E \end{bmatrix}\begin{Bmatrix} \gamma_d \\ \theta \end{Bmatrix}^{t} = \begin{Bmatrix} 0 \\ -F_N \end{Bmatrix}^{t+\frac{1}{2}} + \begin{bmatrix} Y_{Ra}^T[I - A(A+B)^{-1}] \\ -C_2(A+B)^{-1} \end{bmatrix}\{w_g\}^{t+1} + \begin{bmatrix} -Y_{Ra}^T B(A+B)^{-1} \\ -C_1(A+B)^{-1} \end{bmatrix}\{w_g\}^t \tag{18}$$

Numerical Results and Discussions

The mathematical model is a simple delta wing configuration with a leading-edge sweep of 45 deg. The model was constructed from $\frac{3}{32}$-in.-thick plastic (Lucite material) plate. Poisson's ratio is $\nu = 0.45$. A structural modal damping ratio of 0.04 (determined from experiment) was used for all modes.

The theoretical prediction is based on Eq. (18). We use the aerodynamic vortex lattice model including 120 vortex elements on the delta wing ($km = kn = 15$), 525 vortex elements in the wake ($kmm = 50$), and 9 reduced aerodynamic eigenmodes $R_a = 9$. The vortex relaxation factor was taken to be $\alpha = 0.992$ (Ref. 3). The delta wing structural modal numbers were $nxy = 10$ in the out-of-plane and $mxy = 10$ in the in-plane directions, respectively. The mesh of the finite element model for the out-of-plane structural model

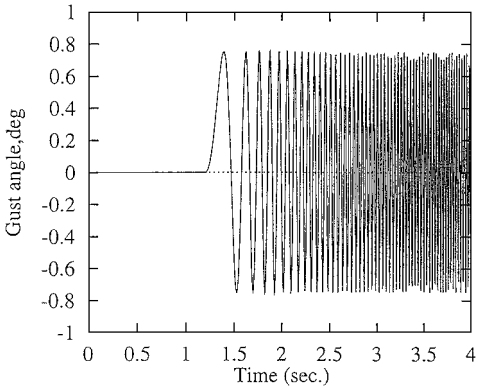

a) Increasing linear frequency sweep process from 0 to 40 Hz

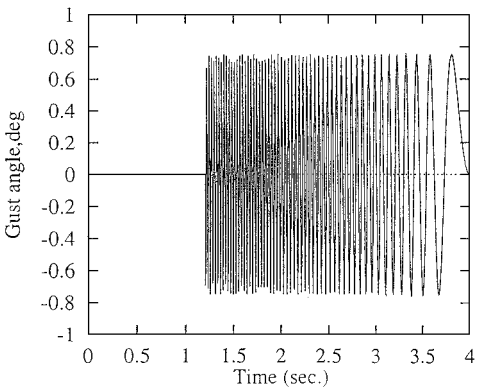

b) Decreasing sweep process

Fig. 2 Theoretical linear frequency sweep time histories.

is 30×30, and thus, the delta wing was modeled using 900 quadrilateral plate elements. The mesh of the three-dimensional finite element model for the in-plane structural model is $30 \times 30 \times 1$, and the delta wing was modeled using 961 solid elements with 1921 nodes. The nodes at the clamped root chord satisfy geometric boundary conditions, that is, $w = u = v = R_x = R_y = R_z = 0$.

The theoretical first 10 natural frequencies are 7.47, 29.61, 33.84, 70.27, 83.78, 107.01, 132.95, 143.91, 153.67, and 180.58 Hz. The theoretical flutter velocity of this model without a gust is 40.25 m/s, and the corresponding flutter frequency ω_F is 21.25 Hz.

The theoretical lateral gust velocity amplitude w_{g0} is 0.75 deg for both single harmonic and linear frequency sweep gust loads. For the latter, the minimum and maximum frequencies are 0 and 40 Hz, and the sweep duration T is 2.8 s, [recall Eq. (8)].

Figures 2a and 2b show the theoretical linear frequency sweep time histories. Figure 2a is an increasing linear frequency sweep process from 0 to 40 Hz and Fig. 2b is a decreasing sweep process.

Results for Flow Velocities Lower Than U_F

A typical frequency-response curve at the measurement point located near the tip of delta wing is shown in Fig. 3 for $U = 20$ m/s obtained from a single harmonic excitation. An rms value is shown because the response is not a pure harmonic motion. When different initial conditions were used, we can obtain two different response amplitudes, as shown by the solid and broken lines. When the excitation frequency continually increases from 0 to 40 Hz, the results are shown by the solid line. The results for decreasing frequency are shown by the broken line. There is a jump response because of the bending/tension or geometrical nonlinearities of the delta wing plate. For comparison, a result from a linear structural model [i.e., $F_N = 0$ in Eq. (18)] is also plotted in Fig. 3, as shown by the dash–dot line. The nonlinear response generally has a higher resonant frequency and smaller amplitude than that for the linear system. Note the resonant frequency of the linear system is 8.5 Hz. From a fast Fourier transform (FFT) analysis, a 3ω frequency component

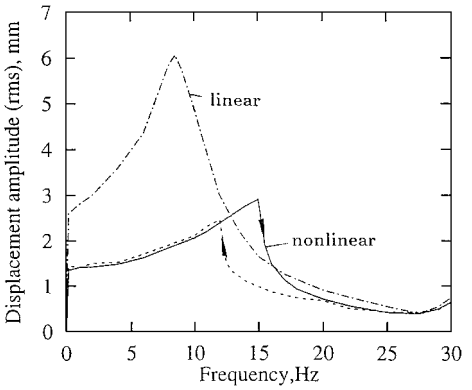

Fig. 3 Frequency response curve to the single harmonic gust excitation for U = 20 m/s.

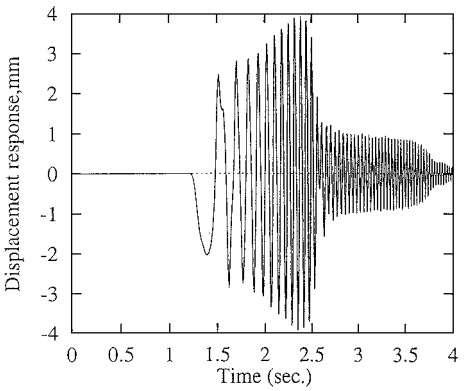

a) Increasing linear frequency sweep process

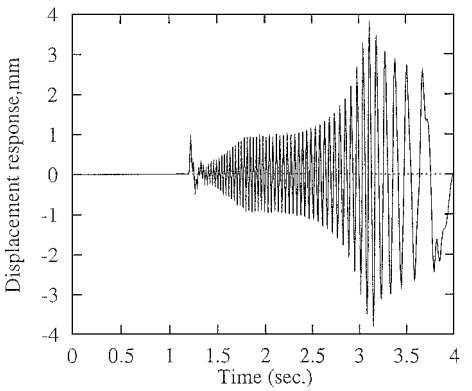

b) Decreasing sweep process

Fig. 4 Gust response time history to a linear frequency sweep gust load, for U = 20 m/s.

response caused by the geometrical nonlinearity is observable (this is not shown in Fig. 3, which is the rms response).

Typical theoretical results for the transverse response near the tip of delta wing to a frequency sweep gust excitation are shown in Figs. 4a and 4b for $U = 20$ m/s. Figure 4a corresponds to an increasing linear frequency sweep gust excitation and Fig. 4b to a decreasing frequency sweep. From the envelope of this time response, there is a jump phenomenon for both gusts, but the time corresponding to the maximum response amplitude is different. One is 2.25 s corresponding to an excitation frequency $\omega = 15$ Hz (Fig. 4a), and the other is 3.19 s corresponding to $\omega = 11.56$ Hz (Fig. 4b). For a linear frequency sweep gust, an instantaneous frequency is defined by

$$\omega = \frac{\mathrm{d}\phi}{\mathrm{d}t} = \omega_1 + \frac{\omega_2 - \omega_1}{T} t \tag{19}$$

To characterize the nonlinear gust response behavior in an approximate way, we form an average envelope from the upper and lower envelope of this time response, and then transfer this averaged envelope to a frequency response curve using Eq. (19), as shown in Fig. 5. The response amplitude is taken as a peak value corresponding to each excitation frequency. The right and left arrows indicate a sweep direction. Compare these results with those in Fig. 3 for a single frequency excitation; the two curves are nearly the same beyond the resonant frequency range. Note in particular they show the same jump trends.

Results for Flow Velocities Higher Than U_F

As is known from Ref. 5, the delta wing model has an LCO when the flow velocities are higher than U_F (without a lateral gust). Now with the gust excitation applied, typical frequency response (rms) curves near the tip of the delta wing are shown by a solid line (increasing frequency excitation) and a broken line (decreasing frequency excitation) in Fig. 6 for $U = 44$ m/s as obtained from a single harmonic excitation. When $\omega = 0$ Hz, the response amplitude is equal to the LCO value and the oscillation frequency is 22.2 Hz. When $\omega = 0.1$ Hz, the vibration behavior is entirely changed, as shown in Fig. 7, where clearly the time history is no longer simple harmonic. Figure 8 shows a typical time history and corresponding FFT for $\omega = 12$ Hz. Again we found there is a detectable 3ω frequency component in addition to a dominant ω component for this nonlinear system.

Similar to Fig. 4, a theoretical result for the transverse response near the tip of delta wing to a frequency sweep gust excitation is shown in Figs. 9a and 9b for $U = 44$ m/s. It is seen that the gust load is initiated at 1.2 s. Before that time, a natural LCO is shown. From an averaged envelope of this time response, a jump phenomenon for both sweep excitations is found. The jump occurs at 2.25 s for Fig. 9a and 3.19 s for Fig. 9b. The instantaneous gust excitation frequencies corresponding to these jump times are $\omega = 25$ and 21.7 Hz. The results are very similar to those for $U = 20$ m/s.

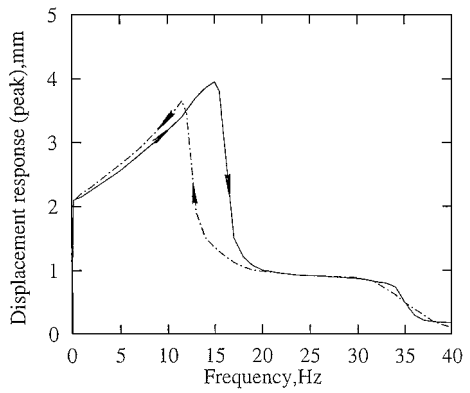

Fig. 5 Envelop behavior of a linear frequency sweep gust load for U = 20 m/s.

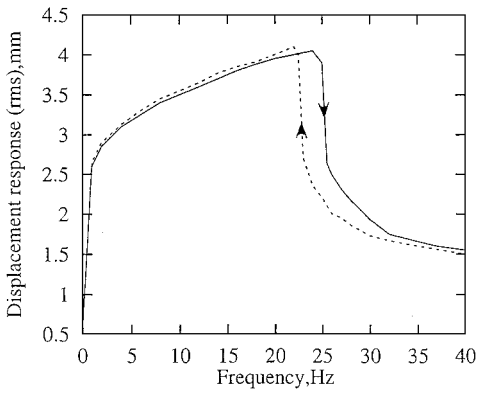

Fig. 6 Frequency response curve to the single harmonic gust excitation for U = 44 m/s.

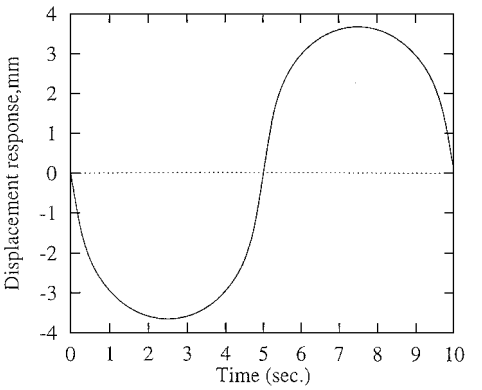

Fig. 7 Time history of gust response to a single harmonic excitation at ω = 0.1 Hz for U = 44 m/s.

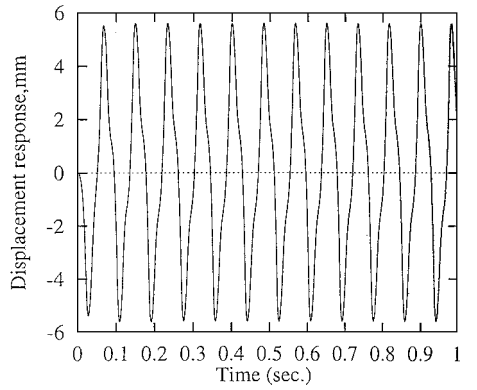

a) Time history

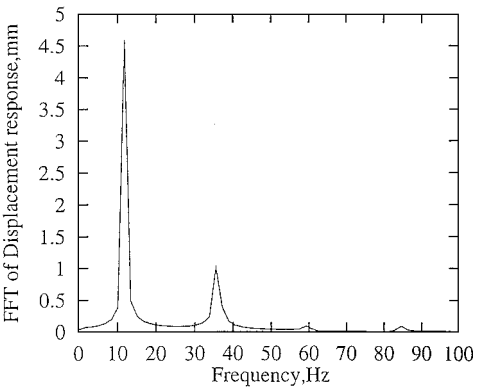

b) FFT analysis

Fig. 8 Gust response to a single harmonic excitation at ω = 12 Hz for U = 44 m/s.

When we decrease the gust strength w_{g0} from 0.75 to 0.1 deg, the natural LCO behavior has a relatively greater influence on the gust response. Figure 10 shows a theoretical result for the transverse response near the tip of the delta wing to the frequency sweep gust excitation for $U = 44$ and $w_{g0} = 0.1$ deg. Comparing Fig. 10 to Fig. 9, we find three differences:

1) The response amplitude becomes smaller for the whole frequency range for the smaller gust excitation.

2) The jump phenomenon at the higher frequency disappears, and the frequency response curves made from an averaged envelope of these time responses are very similar for both the increasing and decreasing linear frequency sweep processes. This means that the smaller gust load is not sufficient to excite a jump response of the nonlinear system.

3) The natural LCO behavior has a larger relative influence in the gust response for the smaller gust excitation.

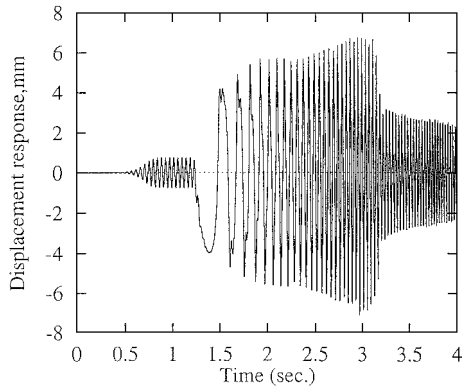

a) Increasing linear frequency sweep process

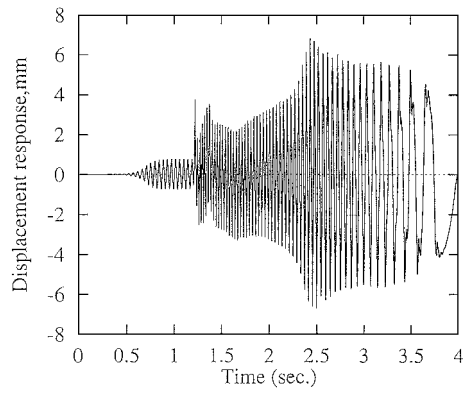

b) Decreasing sweep process

Fig. 9 Gust response time history to a linear frequency sweep gust load, for U = 44 m/s and w_{g0} = 0.75 deg.

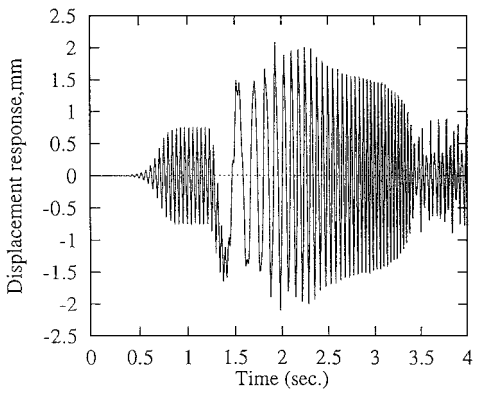

a) Increasing linear frequency sweep process

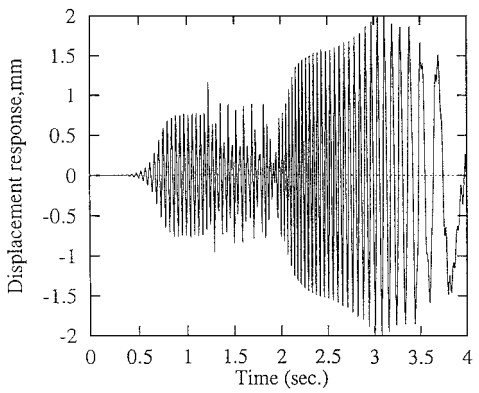

b) Decreasing sweep process

Fig. 10 Gust response time history to a linear frequency sweep gust load, for U = 44 m/s and w_{g0} = 0.1 deg.

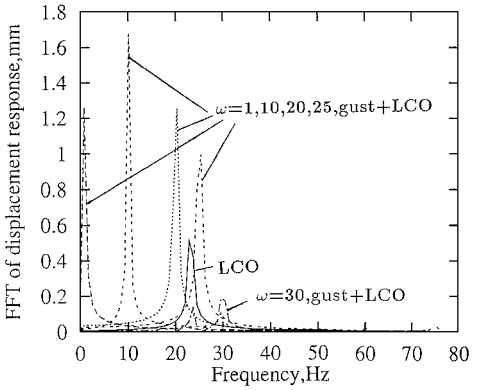

Fig. 11 FFT analysis of gust response to the single harmonic excitation at frequencies ω = 1, 10, 20, 25, and 30 Hz, for U = 44 m/s and w_{g0} = 0.1 deg.

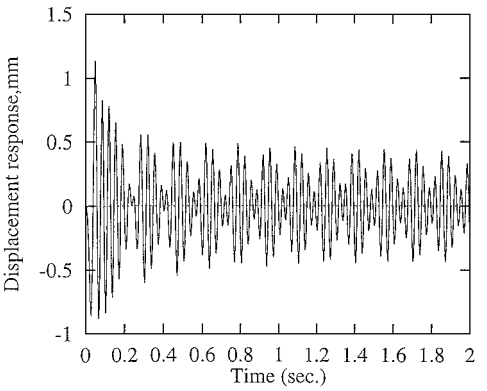

a) Time history

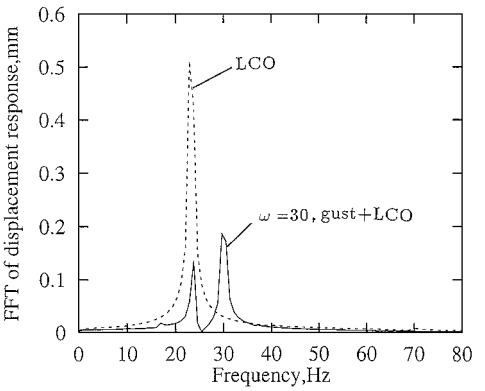

b) FFT analysis

Fig. 12 Gust response to a single harmonic excitation at ω = 30 Hz for U = 44 m/s and w_{g0} = 0.1 deg.

To confirm these results, gust responses to a single harmonic excitation at $\omega = 1$, 10, 20, 25, and 30 have been calculated. The results are shown in Fig. 11 for an FFT analysis of the displacement response. It is found that there is a maximum amplitude at $\omega = 10$ Hz, which corresponds to $t = 1.94$ s in Fig. 10a.

Figure 12 shows the time history and the corresponding FFT analysis for $\omega = 30$ Hz. In Fig. 12b, a dashed line indicates the result from the natural LCO for reference, that is, $\omega = 0$ Hz, and the solid line is for $\omega = 30$ Hz. Also from Fig. 12a we find the time history of response includes a strong LCO component. Note the gust excitation in this case acts to quench or diminish the LCO. Of course, such a result can only occur for a nonlinear system.

To summarize this subsection, Fig. 13 showing nondimensional transverse displacement (rms) near the tip of the delta wing vs flow velocity has been prepared for a range of gust frequency, $\omega = 0$, 1, 10, and 20 Hz and a gust strength of $w_{g0} = 0.75$ deg. For $\omega = 0$, this

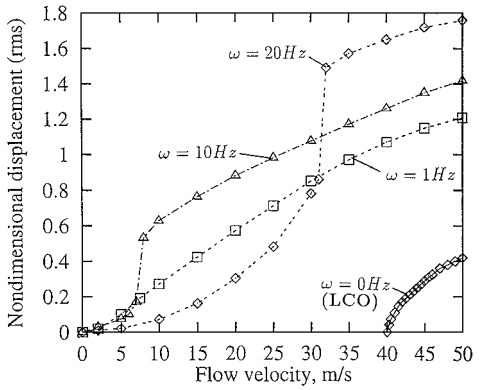

Fig. 13 Nondimensional transverse displacement (rms) vs the flow velocity for gust frequencies ω = 0, 1, 10, and 20 Hz and gust strength w_{g0} = 0.75 deg.

curve indicates a natural LCO as described in Ref. 5. For $\omega = 10$ Hz, the response has a jump at a flow velocity $U = 8$ m/s. For flow velocities lower than $U = 8$ m/s, the gust responses are small, but for larger flow velocities, the gust responses become large and increase with increasing flow velocity. These response amplitudes are larger than the natural LCO amplitude. As the flow velocity increases and exceeds a certain value, the aeroelastic system can undergo nonlinear resonant response due to a dynamic coupling between the aerodynamics and the nonlinear dynamic structural deflection. Thus, a jump phenomenon occurs, and a larger oscillation occurs. These phenomena also occur for higher frequency gust loads, as shown for $\omega = 20$ Hz. Compare the results from $\omega = 10$ Hz to those from $\omega = 20$; the jump velocity ($U = 31$ m/s) and the response amplitude (after the jump) of the latter are larger than those of the former.

Correlation Between Theoretical and Experimental Results

The experimental model has the same parameters as in the numerical example discussed earlier. The root chord was locally clamped (cantilevered), and the length of the cantilever root was 9 in. (60% root chord). The clamping was symmetric about the center of the root chord of the model. The length of the root chord was 15 in. The clamped root of this model is fixed on a root support mechanism that is placed at the top of the tunnel. The delta wing model is mounted in a vertical position in the center of the test section that eliminates gravitational preload in the out-of-plane direction. To avoid the effect of the wind-tunnel body vibration on the model response, the root support mechanism of the model was separated from the ceiling of the tunnel. The mechanism is directly mounted to a heavy support frame that is supported to the ground. The experimental first four natural frequencies are 7.5, 31, 35, and 76 Hz. The agreement with the corresponding theoretical results is good.

The gust was created by placing an RSC behind an airfoil upstream of the delta wing model. The gust generator configuration in the wind tunnel had two airfoils or vanes and two RSCs. The distance between these vanes was 12 in. For details of the gust generator design, see Ref. 6.

Structural response measurements were made using the Ometron VPI 4000 scanning laser vibrometer system.[9] The VPI sensor is a noncontacting transducer that uses optical interferometry and electronic frequency measurements to determine the frequency shift of a beam of light reflected from a moving surface. The system then uses frequency tracking methods to convert the frequency shift to an analog voltage corresponding to the velocity of the moving surface. Because there is no contact between the laser and the delta wing, the system is capable of making point velocity FFT or power spectrum measurements without altering the dynamics of the delta wing or the flow across it. A photograph of the wind-tunnel model, gust generator, and the laser vibrometer system is shown in Fig. 14.

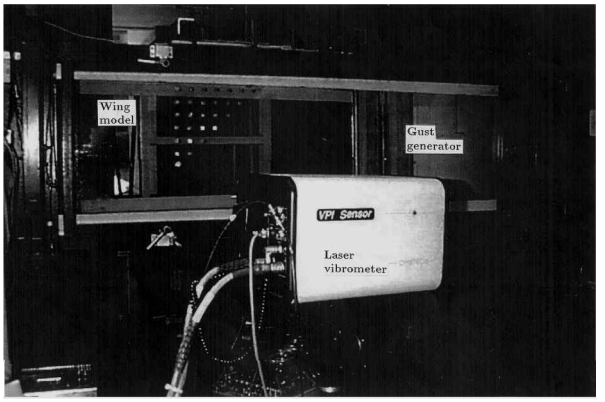

Fig. 14 Wind-tunnel model, gust generator, and the laser vibrometer system.

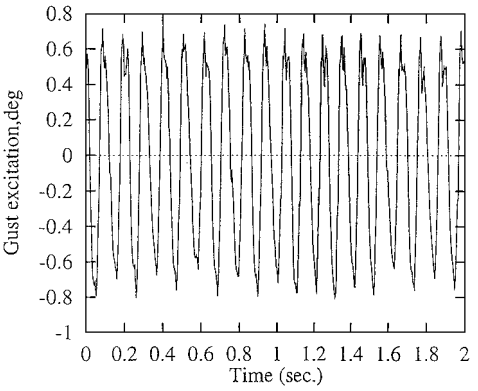

a) Time history

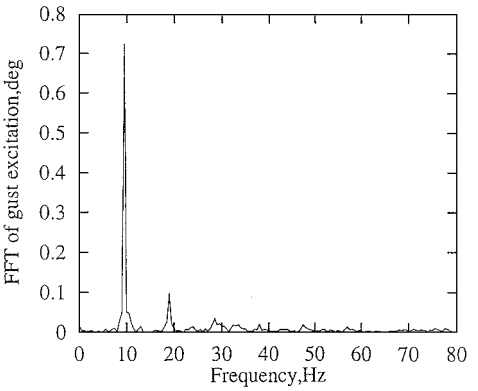

b) FFT

Fig. 15 Lateral gust of single harmonic gust excitation for ω = 9.5 Hz and U = 20 (m/s).

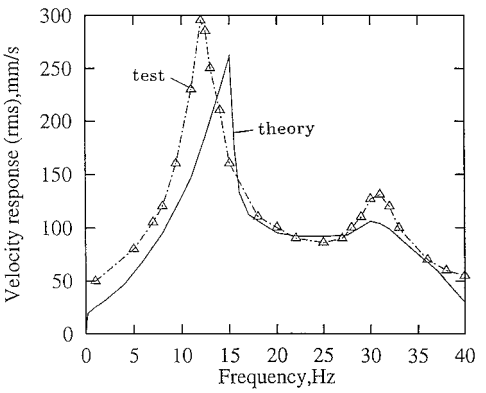

Fig. 16 Velocity frequency response to the single harmonic gust excitation for U = 20 m/s.

Single Harmonic Gust Excitation

A typical measured gust angle (lateral gust wave) generated by the RSC gust generator is shown in Fig. 15a for an airstream velocity of $U = 20$ m/s and cylinder rotation speed of $\omega_s = 5$ Hz. The gust dominant frequency has been shown to be $2\omega_s$. A corresponding FFT plot is shown in Fig. 15b. The gust angle of the first harmonic frequency ($2\omega_s = 10$ Hz) is 0.75 deg, and the second harmonic ($4\omega_s = 20$ Hz) is 0.1 deg. See Ref. 6 for a discussion of gust field measurement.

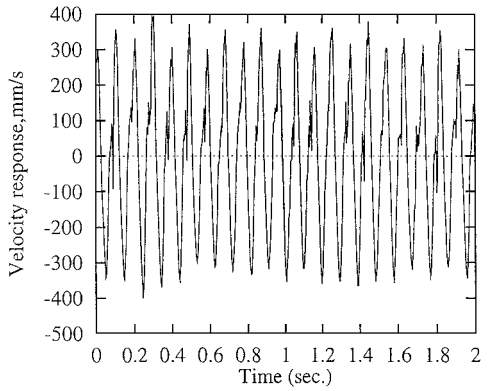

a) Time history

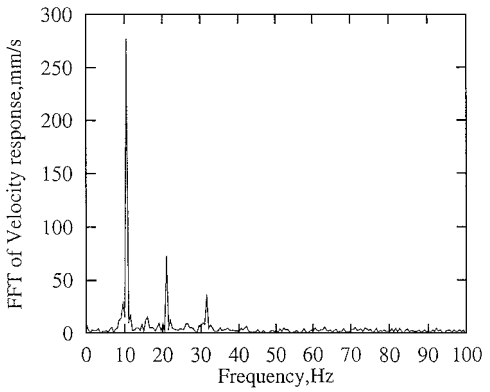

b) FFT

Fig. 17 Measured velocity response to the single frequency gust excitation for ω = 10.5 Hz and U = 20 (m/s).

Figure 16 shows a velocity frequency response curve near the tip of the delta wing for flow velocity $U = 20$ m/s. The theoretical results are shown by a solid line and the experimental results are shown by a dashed line with a △. Note that in Fig. 16 the measured velocity response is not a pure harmonic motion; therefore, we use an average rms method to characterize the response for correlation purposes. The sampling rate is 256 point/s, $\Delta t = 1/256$, and the total sampling length is 600 points. The measured rms velocity $\dot{w}_{\text{rms}}$ is determined from these data. The quantitative agreement is reasonably good. The experimental first resonant frequency is about 12 Hz, which is lower than the theoretical value (15 Hz). This is because the present experimental apparatus does not give a pure tone lateral sinusoidal gust wave. Thus, it is more difficult to obtain an experimental jump phenomenon than if we had a pure single harmonic gust excitation.

Figure 17 shows a typical velocity time response (Fig. 17a) and a corresponding FFT analysis (Fig. 17b). The dominant frequency response component is located at the frequency $\omega = 10.5$ Hz, and there are the detectable 2ω and 3ω frequency components in addition to a dominant ω component for this measured nonlinear system.

Figure 18 shows the vibration shape of the delta model during the steady-state vibration and the correlation between theoretical and experimental nondimensional transverse rms velocity amplitude at $U = 20$ m/s and $\omega = 10$ Hz. The agreement is reasonably good. Note that in the present experiment the measured rms velocity is normalized by $h\omega_F$.

Figure 19 shows the theoretical (solid line) and experimental nondimensional transverse velocity (rms) near the tip of the delta wing vs flow velocity for a range of gust frequencies, $\omega = 0$, 10, and 20 Hz. The broken line with symbols ◇, □, and △ indicate $\omega = 0$, 10, and 20 Hz, respectively, from the experiment. These results show a good agreement between the theory and experiment, although we did not find the predicted theoretical jump phenomenon at $U = 8$ m/s for $\omega = 10$ Hz and at $U = 31$ m/s for $\omega = 20$ Hz. This may also be a result of the experimental gust excitation having multiple frequency components.

Continuous Frequency Sweep Gust Excitation

A continuous lateral gust wave generated by the linear frequency sweep RSC/airfoil experimental system for an airstream velocity of $U = 20$ m/s and a cylinder rotation speed from 0 to 20 Hz, that is, gust excitation frequency from 0 to 40 Hz, is shown in Fig. 20a. There are 10 sweep periods in 34 s, and the total sampling length is

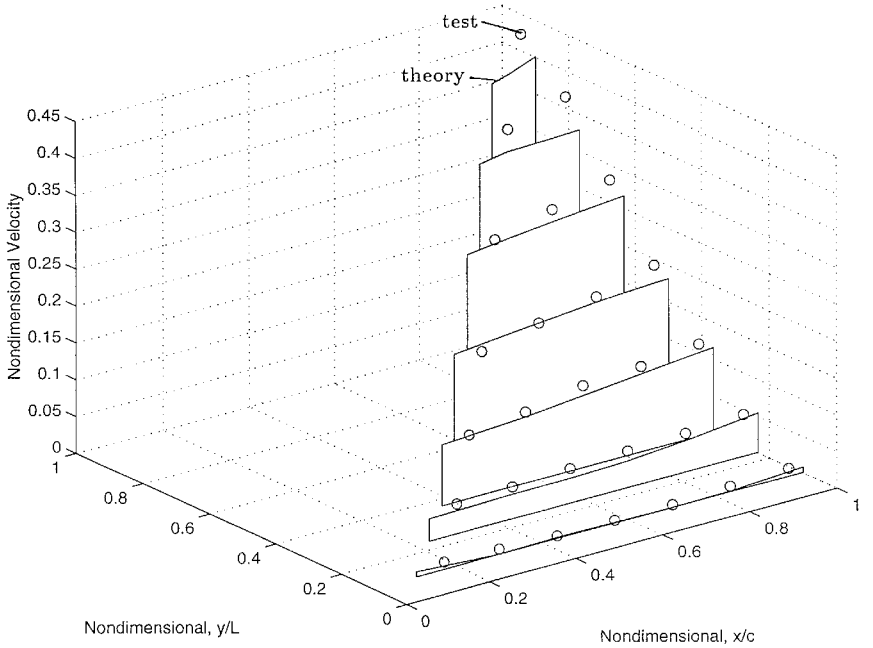

Fig. 18 Vibration shape and correlation between theoretical and experimental nondimensional transverse velocity amplitude for ω = 10.5 Hz and U = 20 m/s.

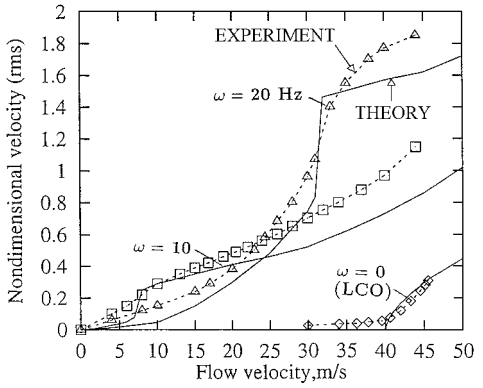

Fig. 19 Theoretical and experimental nondimensional transverse velocity (rms) vs the flow velocity for gust frequencies $\omega = 0, 10$, and 20 Hz.

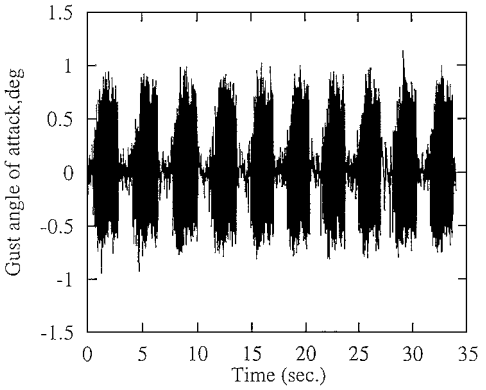

a) Whole time history

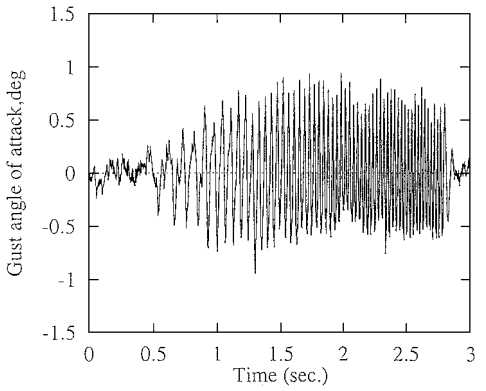

b) One sweep period

Fig. 20 Measured continuous lateral gust of linear frequency sweep gust excitation for $\omega = 0$–40 (Hz) and $U = 20$ (m/s).

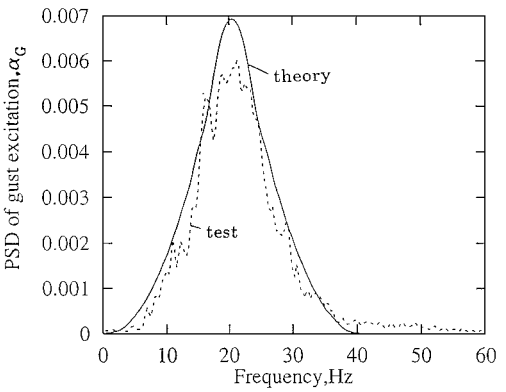

Fig. 21 Theoretical and experimental PSD of the lateral gust excitation.

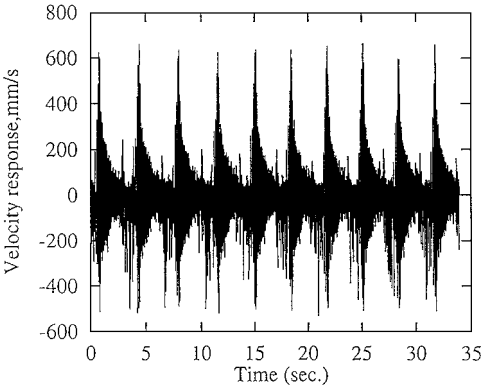

a) Whole time history

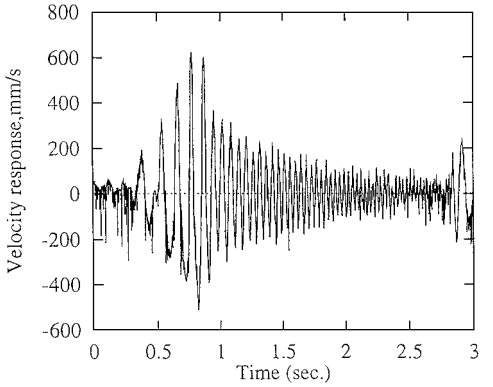

b) One sweep period

Fig. 22 Measured gust response to continuous lateral gust for $U = 20$ (m/s).

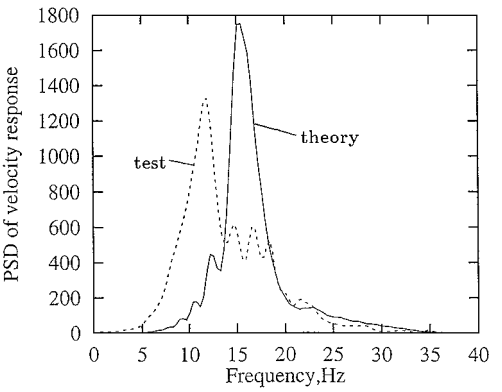

Fig. 23 Theoretical and experimental PSD of the velocity response to the lateral gust excitation for $U = 20$ (m/s).

51,200 points. Figure 20b shows a typical lateral gust wave of one sweep period. The gust wave is not a pure uniform linear frequency sweep. The average angle of the linear frequency sweep gust is about 0.75 deg. It is noted that the measured lateral gust has about a 0.7-s time delay, that is, the restarting time of the dc motor for each repeated cycle. This is due to the rotational inertia of the dc motor. A corresponding power spectra density (PSD) plot is shown by a broken line in Fig. 21, based on an average over 10 sweep periods.

For comparison with the experimental results, a theoretical PSD plot is calculated from a continuous frequency sweep gust excitation (the time history is shown in Fig. 2a) as shown by a solid line of Fig. 21. The result is obtained by using Eq. (8) and one sweep period. The theoretical results (solid line) and the experiment data (broken line) are in reasonably good agreement.

Figure 22 shows a measured velocity response to a continuous lateral gust wave excitation for a flow velocity of $U = 20$ m/s.

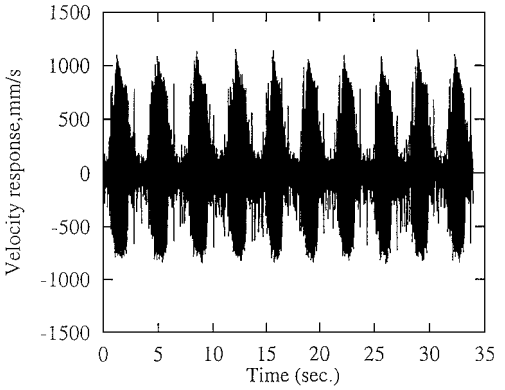

a) Whole time history

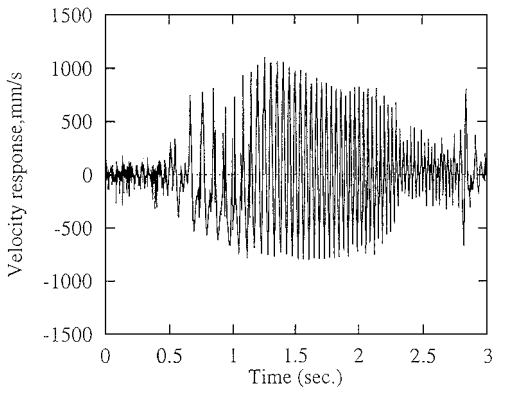

b) One sweep period

Fig. 24 Measured gust response to continuous lateral gust for U = 44 (m/s).

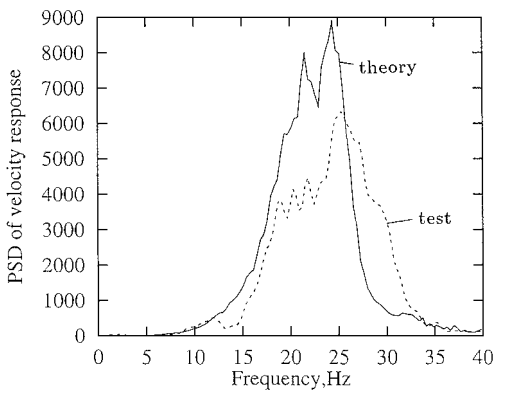

Fig. 25 Theoretical and experimental PSD of the velocity response to the lateral gust excitation for U = 44 (m/s).

Figure 22a is for the first 10 sweep periods, as shown in Fig. 20a, and Fig. 22b is for 1 sweep period. The present experimental results do not verify the theoretical jump phenomenon as shown in Fig. 4a. We believe this is because the experimental gust strength varies with the gust frequency. A corresponding PSD plot is shown by a broken line in Fig. 23 for an average over 10 sweep periods. The theoretical results are shown by a solid line. There is a detectable difference in the location of the peak position (resonant frequency), 15 Hz for the theory and 12 Hz for the experiment. This is consistent with the results obtained for the single harmonic gust excitation as shown in Fig. 16.

Figure 24 shows a measured velocity response to a continuous lateral gust excitation for a flow velocity of $U = 44$ m/s. Figure 24a is for the first 10 sweep periods, and Fig. 24b is for 1 sweep period. A corresponding PSD plot is shown by a broken line in Fig. 25 for an average over 10 sweep periods. The theoretical results are shown by a solid line. There is a resonant frequency at $\omega = 25$ Hz for both the theoretical and experimental results. Note that these results are in the flow velocity range beyond the onset of the LCO for this system.

Results complement previous studies[6,10] of LCD.

Conclusions

A nonlinear response analysis of a delta wing model to periodic and random gust loads in low subsonic flow has been presented. The approach has made use of a three-dimensional time-domain vortex lattice aerodynamic model and a reduced order aerodynamic technique. Results for a single harmonic gust and a continuous frequency sweep gust (modeling a random gust) have been computed and measured both for a lower flow velocity ($U < U_F$) as well as a higher flow velocity ($U > U_F$), where U_F is the flutter velocity. It was shown that the effects of geometric structural nonlinearity due to bending tension for a low aspect ratio plate on the dynamic aeroelastic behavior are significant when an LCO occurs. A theoretical jump response phenomenon for the nonlinear structural model was observed both for the single harmonic and continuous frequency sweep gust excitation. This jump phenomenon was not observed experimentally; possibly the experiment gust excitation was not a pure single harmonic. These results complement our earlier theoretical and experimental studies of LCO.

The fair to good quantitative agreement between theory and experiment verifies that the present method has reasonable accuracy and good computational efficiency for nonlinear gust response analysis in the time domain. Without the use of reduced order models, calculations of the gust response as shown here would be impractical.

Further investigation of the present method should be considered including more general representations of atmospheric turbulence, rather than the special periodic gust that we used here.

Acknowledgments

This work was supported under the U.S. Air Force Office of Scientific Research Grant, "Limit Cycle Oscillations and Nonlinear Aeroelastic Wing Response." C. I. Chang and Brian Sanders are the Grant Program Officers. The authors would also like to thank Robert Clark for his help with implementing the laser measurement system. All numerical calculations were done on a supercomputer, T916, in the North Carolina Supercomputing Center.

References

[1] Jones, J. G., "Statistical Discrete Gust Theory for Aircraft Loads," Royal Aircraft Establishment, TR 73167, London, U.K., Nov. 1973.

[2] Perry, B., III, Pototzky, A. S., and Woods, J. A., "NASA Investigation of a Claimed Overlap Between Two Gust Response Analysis Methods," *Journal of Aircraft*, Vol. 27, No. 7, 1990, pp. 606–611.

[3] Hall, K. C., "Eigenanalysis of Unsteady Flows About Airfoils, Cascades, and Wings," *AIAA Journal*, Vol. 32, No. 12, 1994, pp. 2426–2432.

[4] Dowell, E. H., "Eigenmode Analysis in Unsteady Aerodynamics: Reduced Order Models," *AIAA Journal*, Vol. 34, No. 8, 1996, pp. 1578–1588.

[5] Tang, D. M., Herry, J. K., and Dowell, E. H., "Limit Cycle Oscillations of Delta Wing Models in Low Subsonic Flow," *AIAA Journal*, Vol. 37, No. 11, 1999, pp. 1355–1362.

[6] Tang, D. M., Cizmas, Paul G. A., and Dowell, E. H., "Experiments and Analysis for a Gust Generator in a Wind Tunnel," *Journal of Aircraft*, Vol. 33, No. 1, 1996, pp. 139–148.

[7] Tang, D. M., and Dowell, E. H., "Nonlinear Response of a Non-Rotating Rotor Blade to a Periodic Gust," *Journal of Fluids and Structures*, Vol. 10, No. 7, 1996, pp. 721–742.

[8] Tang, D. M., and Dowell, E. H., "Response of a Nonrotating Rotor Blade to Lateral Turbulence in Sinusoidal Pulsating Flow, Part 2: Experiment," *Journal of Aircraft*, Vol. 32, No. 1, 1995, pp. 154–160.

[9] "VPI 4000 Scanning Laser Vibrometer Operator's Manual," Ometron, Sterling, VA, July 1997.

[10] Tang, D. M., Dowell, E. H., and Hall, K. C., "Limit Cycle Oscillations of a Cantilevered Wing in Low Subsonic Flow," *AIAA Journal*, Vol. 37, No. 3, 1999, pp. 364–371.